

# Minimal Paths in 3D Images and Application to Virtual Endoscopy

Thomas Deschamps<sup>1,2</sup> and Laurent D. Cohen<sup>2</sup>

<sup>1</sup> Medical Imaging Systems Group, LEP,

22, avenue Descartes, BP 15, 94453 Limeil-Brévannes Cedex, France  
deschamp@lep-philips.fr, Telephone : 33-1-45 10 68 56, Fax : 33-1-45 10 69 59

<sup>2</sup> Université Paris IX Dauphine, CEREMADE UMR CNRS 7534,

Place du Marechal de Lattre de Tassigny, 75775 Paris Cedex 16, France  
cohen@ceremade.dauphine.fr, Telephone : 33-1-44 05 46 78, Fax : 33-1-44 05 45 99

**Abstract.** This paper presents a new method to find minimal paths in 3D images, giving as initial data one or two endpoints. This is based on previous work [1] for extracting paths in 2D images using Fast Marching [4]. Our original contribution is to extend this technique to 3D, and give new improvements of the approach that are relevant in 2D as well as in 3D. We also introduce several methods to reduce the computation cost and the user interaction.

This work finds its motivation in the particular case of 3D medical images. We show that this technique can be efficiently applied to the problem of finding a centered path in tubular anatomical structures with minimum interactivity, and we apply it to path construction for virtual endoscopy. Synthetic and real medical images are used to illustrate each contribution.

**keywords** : Deformable Models, Minimal paths, Level Set methods, Medical image understanding, Eikonal Equation, Fast Marching.

## 1 Introduction

In this paper we deal with the problem of finding a curve of interest in a 3D image. It is defined as a minimal path with respect to a Potential  $P$ . This potential is derived from the image data depending on which features we are looking for.

With classical deformable models [2], extracting a path between two fixed extremities is the solution of the minimization of an energy composed of internal and external constraints on this path, needing a precise initialization. Similarly, defining a cost function as an image constraint only, the minimal path becomes the path for which the integral of the cost between the two end points is minimal. Simplifying the model to external forces only, Cohen and Kimmel [1] solved this minimal path problem in 2D with a front propagation equation between the two fixed end points, using the *Eikonal* equation (that physically models wavelight propagation), with a given initial front. Therefore, the first step is to build an image-based measure  $P$  that defines the minimality property in the studied image, and to introduce it in the *Eikonal* equation. The second step is to propagate the front on the entire image domain, starting from an initial front restricted to one of the fixed points. The propagation is done using an algorithm called *Fast Marching* [4].

The original contribution of our work is to adapt to 3D images the minimal path technique developed in [1]. We also improve this technique by reducing the computing cost of front propagation. For the particular case of tubular anatomical structures, we

also introduce a method to compute a path with a given length with only one point as initialization, and another method to extract a centered path in the object of interest.

Deformable models have been widely used in medical imaging [7]. The main motivation of this work is that it enables almost automatic path tracking routine in 3D medical images for virtual endoscopy inside an anatomical object. An endoscopy consists in threading a camera inside the patient’s body in order to examine a pathology. The virtual endoscopy process consists in rendering perspective views along a user-defined trajectory inside tubular structures of human anatomy with CT or MR 3D images. It is a non-invasive technique which is very useful for learning and preparing real examinations, and it can extract diagnostic elements from images. This new method skips the camera and can give views of region of the body difficult or impossible to reach physically (e.g. brain vessels). A major drawback in general remains when the user must define all path points manually. For a complex structure (small vessels, colon,...) the required interactivity can be very tedious. If the path is not correctly built, it can cross an anatomical wall during the virtual fly-through.

Our work focuses on the automation of the path construction, reducing interactions and improving performance, given only one or two end points as inputs. We show that the Fast Marching method can be efficiently applied to the problem of finding a path in virtual endoscopy with minimum interactivity. We also propose a range of choices for finding the right input potential  $P$ .

In section 2, we summarize the method detailed in [1] for 2D images. In section 3, we extend this method to 3D, and we detail each improvement made on the front propagation technique. In section 4, we explain how to extract centered paths in tubular structures. And in section 5, we apply our method to colon and brain vessels.

## 2 The Cohen-Kimmel Method in 2D

### 2.1 Global Minimum for Active Contours.

We present in this section the basic ideas of the method introduced by Cohen and Kimmel (see [1] for details) to find the global minimum of the active contour energy using minimal paths. The energy to minimize is similar to classical deformable models (see [2]) where it combines smoothing terms and image features attraction term (Potential  $P$ ):

$$E(C) = \int_{\Omega} \left\{ w_1 \|C'(s)\|^2 + w_2 \|C''(s)\|^2 + P(C(s)) \right\} ds . \quad (1)$$

where  $C(s)$  represents a curve drawn on a 2D image,  $\Omega$  is its domain of definition  $[0, L]$ , and  $L$  is the length of the curve. It reduces the user initialization to giving the two end points of the contour  $C$ . In [1], the authors have related this problem to the new paradigm of the level-set formulation. In particular, its Euler equation is equivalent to the geodesic active contours [8]. They introduced a model which improves energy minimization because the problem is transformed in a way to find the global minimum, avoiding being stucked in local minima.

Most of the classical deformable contours have no constraint on the parameterization  $s$ , thus allowing different parameterization of the contour  $C$  to lead to different

results. In [1], contrary to the classical snake model (but similarly to geodesic active contours),  $s$  represents the arc-length parameter. Considering a simplified energy model without a second derivative term leads to the expression

$$E(C) = \int_{\Omega} \{w + P(C(s))\} ds . \quad (2)$$

We now have an expression in which the internal forces are included in the external potential. The regularization is now achieved by the constant  $w > 0$ .

Given a potential  $P > 0$  that takes lower values near desired features, we are looking for paths along which the integral of  $\tilde{P} = P + w$  is minimal. We can define the surface of minimal action  $U$ , as the minimal energy integrated along a path between a starting point  $p_0$  and any point  $p$ :

$$U(p) = \inf_{\mathcal{A}_{p_0,p}} E(C) = \inf_{\mathcal{A}_{p_0,p}} \left\{ \int_{\Omega} \tilde{P}(C(s)) ds \right\} . \quad (3)$$

where  $\mathcal{A}_{p_0,p}$  is the set of all paths between  $p_0$  and  $p$ . The minimal path between  $p_0$  and any point  $p_1$  in the image can be easily deduced from this action map. Assuming that potential  $P$  is always positive, the action map will have only one local minimum which is the starting point  $p_0$ , and the minimal path will be found by a simple back-propagation on the energy map. Thus, contour initialization is reduced to the selection of the two extremities of the path.

## 2.2 Fast Marching Resolution.

In order to compute this map  $U$ , a front-propagation equation related to equation (3) is solved:  $\frac{\partial C}{\partial t} = \frac{1}{P} \vec{n}$ . It evolves a front starting from an infinitesimal circle shape around  $p_0$  until each point inside the image domain is assigned a value for  $U$ . The value of  $U(p)$  is the time  $t$  at which the front passes over the point  $p$ . Then it notifies the shortest path energy to reach the start point from any point in the image.

The fast marching technique, introduced by Sethian (see [4]), was used by Cohen and Kimmel [1] noticing that the map  $U$  satisfies the Eikonal equation:

$$\|\nabla U\| = \tilde{P} . \quad (4)$$

Classic finite difference schemes for this equation tend to overshoot and are unstable. Sethian [4] has proposed a method which relies on a one-sided derivative that looks in the up-wind direction of the moving front, and thereby avoids the over-shooting of finite differences. At each pixel  $(i, j)$ , the unknown  $u$  satisfies:

$$\begin{aligned} & (\max\{u - U_{i-1,j}, u - U_{i+1,j}, 0\})^2 + \\ & (\max\{u - U_{i,j-1}, u - U_{i,j+1}, 0\})^2 = \tilde{P}_{i,j}^2 . \end{aligned} \quad (5)$$

giving the correct viscosity-solution  $u$  for  $U_{i,j}$ . The improvement made by the *Fast Marching* is to introduce order in the selection of the grid points. This order is based on the fact that information is propagating *outward*, because action can only grow due to

the quadratic equation (5).

The algorithm is detailed in 3D in next section in table 2. The *fast marching* technique selects at each iteration the *Trial* point with minimum action value. This technique of considering at each step only the necessary set of grid points was originally introduced for the construction of minimum length paths in a graph between two given nodes in [6].

Thus it needs only one pass over the image. To perform efficiently these operations in minimum time, the *Trial* points are stored in a min-heap data structure (see details in [4]). Since the complexity of the operation of changing the value of one element of the heap is bounded by a worst-case bottom-to-top proceeding of the tree in  $O(\log_2 N)$ , the total work is about  $O(N \log_2 N)$  for the *fast marching* on a  $N$  points grid.

### 3 3D Minimal Path Extraction

We are interested in this paper in finding a curve in a 3D image. The application that motivates this problem is detailed in section 5. It can also have many other applications. Our approach is to extend the minimal path method of previous section to finding a path  $C(s)$  in a 3D image minimizing the energy:

$$\int_{\Omega} \tilde{P}(C(s)) ds . \quad (6)$$

where  $\Omega = [0, L]$ ,  $L$  being the length of the curve. We first extend the Fast marching method to 3D to compute the minimal action  $U$ . We then introduce different improvements for finding the path of minimal action between two points in 2D as well as in 3D. In the examples that illustrate the approach, we see various ways of defining the potential  $P$ .

#### 3.1 3D Fast-Marching

Similarly to previous section, the minimal action  $U$  is defined as

$$U(p) = \inf_{\mathcal{A}_{p_0,p}} \left\{ \int_{\Omega} \tilde{P}(C(s)) ds \right\} . \quad (7)$$

where  $\mathcal{A}_{p_0,p}$  is now the set of all 3D paths between  $p_0$  and  $p$ . Given a start point  $p_0$ , in order to compute  $U$  we start from an initial infinitesimal front around  $p_0$ . The 2D scheme equation (5) developed in [5] is extended to 3D, leading to :

$$\begin{aligned} & (\max\{u - U_{i-1,j,k}, u - U_{i+1,j,k}, 0\})^2 + \\ & (\max\{u - U_{i,j-1,k}, u - U_{i,j+1,k}, 0\})^2 + \\ & (\max\{u - U_{i,j,k-1}, u - U_{i,j,k+1}, 0\})^2 = \tilde{P}_{i,j,k}^2 . \end{aligned} \quad (8)$$

giving the correct viscosity-solution  $u$  for  $U_{i,j,k}$ . Considering the neighbors of grid point  $(i, j, k)$  in 6-connexity, we study the solution of the equation (8) in table 1.

We extend the Fast Marching method, introduced in [4] and used by Cohen and Kimmel [1] to our 3D problem. The algorithm is detailed in table 2.

**Algorithm for 3D Up-Wind Scheme**

We note  $\{A_1, A_2\}$ ,  $\{B_1, B_2\}$  and  $\{C_1, C_2\}$  the three couples of opposite neighbors of  $\{i, j, k\}$  with the ordering  $U_{A_1} \leq U_{A_2}$ ,  $U_{B_1} \leq U_{B_2}$ ,  $U_{C_1} \leq U_{C_2}$ , and  $U_{A_1} \leq U_{B_1} \leq U_{C_1}$ . Three different cases are to be examined sequentially:

1. Considering that we have  $u \geq U_{C_1} \geq U_{B_1} \geq U_{A_1}$ , the equation derived is

$$(u - U_{A_1})^2 + (u - U_{B_1})^2 + (u - U_{C_1})^2 = \tilde{P}^2. \quad (9)$$

Computing the discriminant  $\Delta_1$  of equation (9) we have two cases

- If  $\Delta_1 \geq 0$ ,  $u$  should be the largest solution of equation (9);
  - If the hypothesis  $u > U_{C_1}$  is wrong, go to 2;
  - If this value is larger than  $U_{C_1}$ , go to 4;
- If  $\Delta_1 < 0$ , it means that at least  $C_1$  has an action too large to influence the solution and that the hypothesis  $u > U_{C_1}$  is false. Go to 2;

2. Considering that  $u \geq U_{B_1} \geq U_{A_1}$  and  $u < U_{C_1}$ , the equation derived is

$$(u - U_{A_1})^2 + (u - U_{B_1})^2 = P^2. \quad (10)$$

Computing the discriminant  $\Delta_2$  of equation (10) we have two cases

- If  $\Delta_2 \geq 0$ ,  $u$  should be the largest solution of equation (10);
  - If the hypothesis  $u > U_{B_1}$  is wrong, go to 3;
  - If this value is larger than  $U_{B_1}$ , go to 4;
- If  $\Delta_2 < 0$ ,  $B_1$  has an action too large to influence the solution. It means that  $u > U_{B_1}$  is false. Go to 3;

3. Considering that  $u < U_{B_1}$  and  $u \geq U_{A_1}$ , we finally have  $u = U_{A_1} + P$ . Go to 4;
4. Return  $u$ .

**Table 1.** Solving locally the upwind scheme

**Algorithm for 3D Fast Marching**

- Definition:
  - *Alive* is the set of all grid points at which the action value has been reached and will not be changed;
  - *Trial* is the set of next grid points to be examined and for which an estimate of  $U$  has been computed using algorithm of Table 1;
  - *Far* is the set of all other grid points, for which there is not yet an estimate for  $U$ ;
- Initialization:
  - *Alive* set is confined to the starting point  $p_0$ ;
  - *Trial* - the initial front is confined to the neighbors of  $p_0$ ;
  - *Far* is the set of all other grid points;
- Loop:
  - Let  $(i_{min}, j_{min}, k_{min})$  be the *Trial* point with the smallest action  $U$ ;
  - Move it from the *Trial* to the *Alive* set (i.e.  $U_{i_{min}, j_{min}, k_{min}}$  is frozen);
  - For each neighbor  $(i, j, k)$  (6-connexity in 3D) of  $(i_{min}, j_{min}, k_{min})$ :
    - \* If  $(i, j, k)$  is *Far*, add it to the *Trial* set and compute  $U$  using table 1;
    - \* If  $(i, j, k)$  is *Trial*, recompute the action  $U_{i,j,k}$ , and update it if the new value computed is smaller.

**Table 2.** Fast marching algorithm

### 3.2 Several Minimal Path Extraction Techniques

In this section, different procedures to obtain the minimal path between two points are detailed. After discussing the previous backpropagation method, we study how we can limit the front propagation to a subset of the image domain, for speeding-up execution. We illustrate the ideas of this section on two synthetic examples of 3D front propagation in figures 1 and 3. To make the following ideas easier to understand, we show examples in 2D in this section. Examples of minimal paths in 3D real images are presented for the application in Section 5.

**Minimal path by back-propagation** The minimal action map  $U$  computed according to the discretization scheme of equation (7) is similar to convex, in the sense that its only local minimum is the global minimum found at the front propagation start point  $p_0$  where  $U(p_0) = 0$ . The gradient of  $U$  is orthogonal to the propagating fronts since these are its level sets. Therefore, the minimal action path between any point  $p$  and the start point  $p_0$  is found by sliding back the map  $U$  until it converges to  $p_0$ . It can be done with a simple steepest gradient descent, with a predefined descent step, on the minimal action map  $U$ , choosing  $p_{n+1} = p_n - \text{step} \times \nabla U(p_n)$ . See in figure 1-middle the action map corresponding to a binarized potential defined by high values in a spiral rendered in figure 1-middle. The path found between a point in the center of the spiral and another point outside is shown in figure 1-right by transparency.

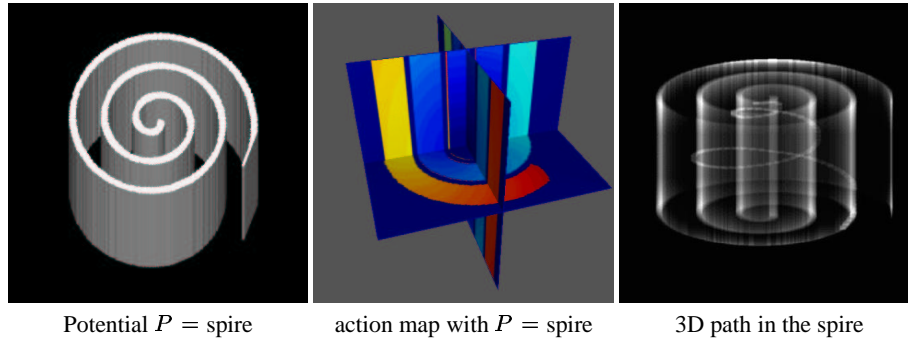
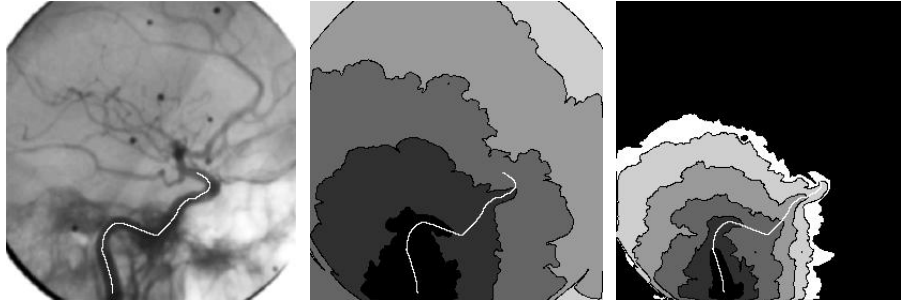


Fig. 1. Examples on synthetic potentials

**Partial front propagation.** An important issue concerning the back-propagation technique is to constrain the computations to the necessary set of pixels for one path construction. Finding several paths inside an image from the same seed point is an interesting task, but in the case we have two fixed extremities as input for the path construction, it is not necessary to propagate the front on all the image domain, thus saving computing time. In figure 2 is shown a test on an angiographic image of brain vessels. We can see that there is no need to propagate further the points examined in figure 2-right, the path found being exactly the same as in figure 2-middle where front propagation is

done on all the image domain. We used a potential  $P(\mathbf{x}) = |\nabla G_\sigma * I(\mathbf{x})| + w$ , where  $I$  is the original image ( $512^2$  pixels, displayed in figure 2-left),  $G_\sigma$  a Gaussian filter of variance  $\sigma = 2$ , and  $w = 1$  the weight of the model. In figure 2-right, the partial front propagation has visited less than 35% of the image. This ratio depends mainly on the length of the path tracked.



**Fig. 2.** Comparing complete front propagation with partial front propagation method on a digital subtracted angiography (DSA) image

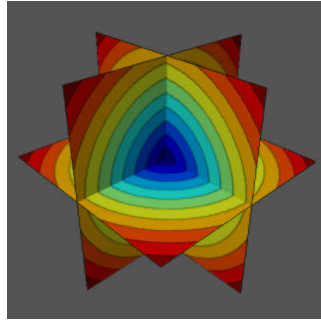
**Simultaneous partial front propagation** The idea is to propagate simultaneously a front from each end point  $p_0$  and  $p_1$ . Lets consider the first grid point  $p$  where those fronts collide. Since during propagation the action can only grow, propagation can be stopped at this step. Adjoining the two paths, respectively between  $p_0$  and  $p$ , and  $p_1$  and  $p$ , gives an approximation of the exact minimal action path between  $p_0$  and  $p_1$ . Since  $p$  is a grid point, the exact minimal path might not go through it, but in its neighborhood. Basically, it exists a real point  $p^*$ , whose nearest neighbor on the Cartesian grid belongs to the minimal path. Therefore, the approximation done is sub-pixel and there is no need to propagates further.

It has two interesting benefits for front propagation:

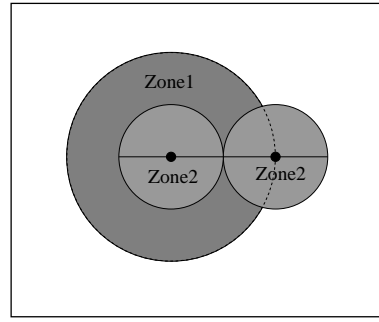
- It allows a parallel implementation of the algorithm, dedicating a processor to each propagation;
- It decreases the number of pixels examined during a partial propagation by
  - $\frac{(2R)^2}{2 \times R^2} = 2$  in 2D (figure 3-right);
  - $\frac{(2R)^3}{2 \times R^3} = 4$  in 3D (figure 3-left).
 because with the potential  $P = 1$ , the action map is the Euclidean distance.

Note that it can also compute the Euclidean distance to a set of points by initializing  $U$  to be 0 at these points.

In figure 4 is displayed a test on a digital subtracted angiography (DSA) of brain vessels. The potential used is  $P(\mathbf{x}) = |I(\mathbf{x}) - C| + w$ , where  $I$  is the original image ( $256^2$  pixels, displayed in figure 4-left),  $C$  a constant term (mean value of the start and end points gray levels), and  $w = 10$  the weight of the model. In figure 4-middle, the partial front propagation has visited up to 60% of the image. With a colliding fronts method, only 30% of the image is visited (see figure 4-right), and the difference between both paths found is sub-pixel.



Action map with potential  $P = 1$



Comparing both methods on potential  $P = 1$

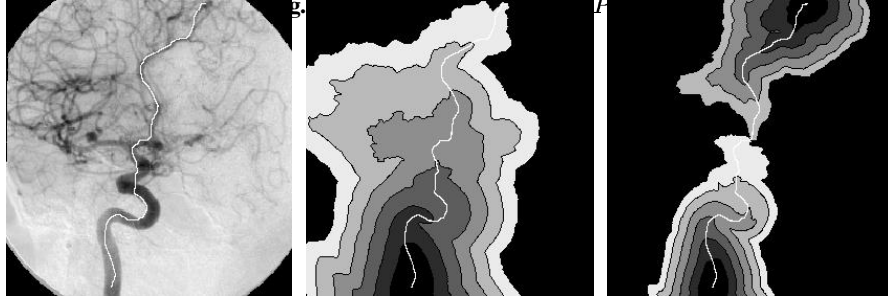


**Fig. 4.** Comparing the partial front propagation with the colliding fronts method on a DSA image

**One end point propagation** We have shown the ability of the front propagation techniques to compute the minimal path between two fixed points. In some cases, only one point should be necessary, or the needed user interaction for setting a second point is too tedious in a 3D image. We have derived a method that builds a path given only one end point and a maximum path length. The technique is similar to that of subsection 3.2, but the new condition will be to stop propagation when a path corresponding to a chosen Euclidean distance is extracted. A test of this path length condition is shown on figure 5 which is a DSA image of brain vessels. We have seen with figure 3-left that propagating a front with potential  $P = 1$  computes the Euclidean distance to the start point. Therefore, we use simultaneously an image-based potential  $P_1$ , for building the minimal path and a potential  $P_2 = 1$  for computing the path length.

While we are propagating the front corresponding to  $P_1$  on the image domain, at each point  $p$  examined we compute both minimal actions for  $P_1$  (shown in figure 5-middle) and for  $P_2$  (shown in figure 5-right). In this case the action corresponding to  $P_2$  is an approximate Euclidean length **of the minimal path** between  $p$  and  $p_0$ .

#### 4 The Path Centering Method

In this section we derive a technique to track paths that are centered in a tubular shape, using the front propagation methods. To illustrate this problem, we use the example shown on figure 6-left, which is a binarized image of brain vessels. Using our classical



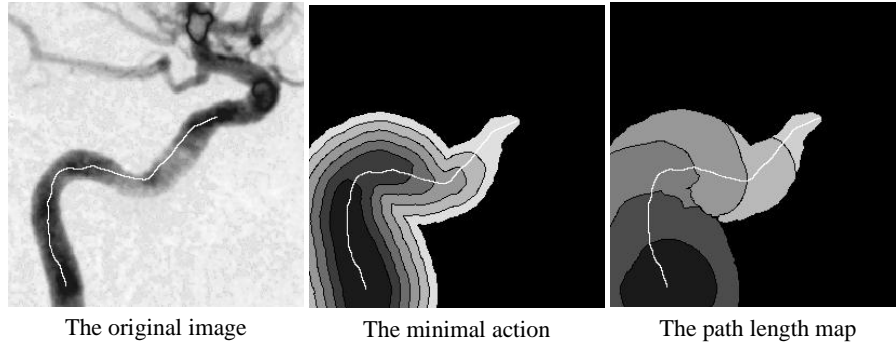


**Fig. 5.** Computing the Euclidean path length simultaneously

front propagation, the minimal path extracted is tangential to the edges, as shown in figure 6-middle, superimposed on the action map computed. This is due to the fact that length is minimized. This path is not tuned for problems which may require a centered path, and we will see in next section that it can be necessary for virtual endoscopy. In

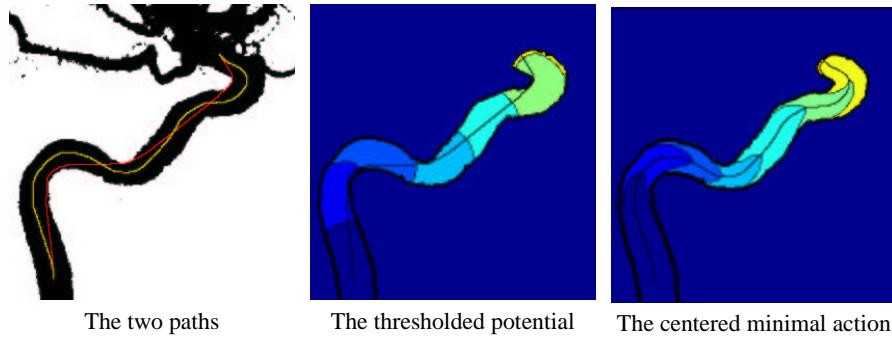


**Fig. 6.** Comparing classic and centered paths

some cases it is possible to get the shape of the object in which we are looking for a path. One way of making this shape available is to use the front propagation itself as shown in Figure 9. This is more detailed in [9]. If we have the shape of our object, we can use a front propagation method to compute the distance to its edges using a potential defined by

$$\begin{aligned}
 P(i, j) &= 1 \quad \forall (i, j) \in \{\text{object}\} . \\
 P(i, j) &= \infty \quad \forall (i, j) \in \{\text{Background}\} . \\
 P(i, j) &= 0 \quad \forall (i, j) \in \{\text{Interface}\} .
 \end{aligned}$$

When this distance map, noted  $\mathcal{E}$ , is computed, it is used to create a potential  $P'$  which weights the points in order to propagate faster a new front in the centre of the desired regions. Choosing a value  $d$  to be the minimum acceptable distance to the walls, we

propose the following potential:

$$P'(\mathbf{x}) = \{|d - \min(\mathcal{E}(\mathbf{x}); d)|\}^\gamma \text{ with } \gamma \geq 1. \quad (11)$$

According to this new penalty, the final front propagates faster in the center of the vessel. This can be observed by looking at the shape of the iso-action lines of the centered minimal action shown in figure 6-right. Finally, one can observe in figure 6-left that the path avoids the edges and remains in the center of the vessel, while the former path tangential to edges. This method can be related to robotic problems like optimal path planning (see [4] for details), essentially because the potential shown in figure 6-left is binary. But there is no reason to limit the application of this algorithm to a binary domain. Thus, for continuously varying potential  $P$ , we use the same method. In section 5, we present results on real 3D data applied to virtual endoscopy, where the problem is to find shortest paths on weighted domains.

## 5 Application to Virtual Endoscopy

In previous sections we have developed a series of issues in front propagation techniques. We study now the particular case of virtual endoscopy, where extraction of paths in 3D images is a very tedious task.

### 5.1 The Role of Virtual Endoscopy

Visualization of volumetric medical image data plays a crucial part for diagnosis and therapy planning. The better the anatomy and the pathology are understood, the more efficiently one can operate with low risk. Different possibilities exist for visualizing 3D data: three 2D orthogonal views (see figure 7), maximum intensity projection (MIP, and its variants), surface and volume rendering. In particular, virtual endoscopy allows

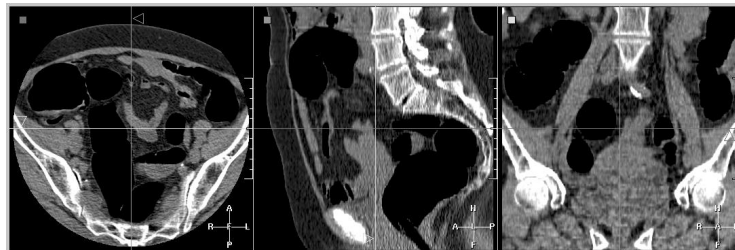


**Fig. 7.** Three orthogonal views of a volumetric CT data set of the colon

by means of surface/volume rendering techniques to visually inspect regions of the body that are dangerous and/or impossible to reach physically with a camera. A virtual endoscopic system is usually composed of two parts:

1. A Path construction part, which provides the successive locations of the fly-through the tubular structure of interest (see figure 8-left);

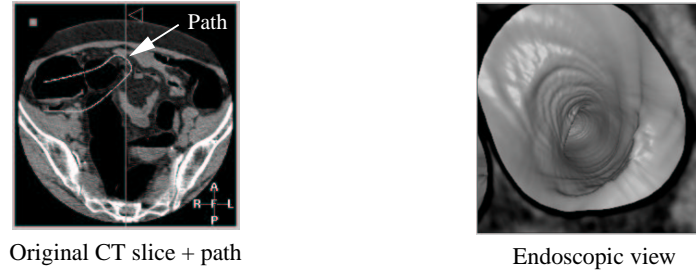


**Fig. 8.** Interior view of a colon, reconstructed from a defined path

2. Three dimensional viewing along the endoscopic path (see figure 8-right).

A major drawback in general remains when the path construction is left to the user who manually has to “guide” the virtual endoscope/camera. The required interactivity on a 3D image can be very tedious for complex structures such as the colon. Since the anatomical objects have often complex topologies, the path passes in and out of the three orthogonal planes. Consequently the right location is accomplished by alternatively entering the projection of the wanted point in each of the three planes. Then, the path is approximated between the user defined points by lines or Bezier splines, and if the number of points is not enough, it can easily cross an anatomical wall. Path construction in 3D images is thus a very critical task and precise anatomical knowledge of the structure is needed to set a suitable trajectory, with the minimum required interactivity.

Numerous techniques [10],[11] try to automate this path construction process by using a skeletonization technique as a pre-processing. It requires first to segment the object in order to binarize the image, then it extracts the skeleton of this volume. The skeleton often consists in lots of discontinuous trajectories, and post-processing is necessary to isolate and smooth the final path. But those methods can lead to critical cases: if there is a stenosis in the tubular structure, the binarization can produce two separate objects, where a skeletonization is inefficient. The front propagation techniques studied in this paper propose an alternative to the tedious manual path construction by building paths in 3D images with minimum interactivity. In contrast to other methods, it does not require any pre- or post-processing. We first apply this method to the case of virtual endoscopy in a colon CT dataset, then we extend it to a brain MR dataset.

## 5.2 Application to Colonoscopy

All tests are performed on a volumetric CT scan of size  $512 \times 512 \times 140$  voxels, shown in figure 7. We define a potential  $P$  from the 3D image  $I(x)$  that is minimal inside the anatomical shapes where end points are located. We chose the potential  $P(x) = |I(x) - I_{mean}|^\alpha + w$ , where an average grey level value  $I_{mean}$  of the colon is obtained with an histogram. From this definition,  $P$  is lower inside the colon in order to propagate the front faster. Also, edges are enhanced with a non-linear function ( $\alpha > 1$ ) since the path to be extracted is in a large object that has complex shape and very thin edges.

Then, using this potential, we propagate inside the colon creating a path between a couple of given points. In fact, the colon being a closed object with two extremities, one can use the Euclidean path length stopping criterion as explained in subsection 3.2. This allows to give only one end point. The figure 9 shows the result of the fast marching technique with a unique starting point belonging to the colon and an Euclidean path length criterion of 500 mm. This path has been computed in 10 seconds (in CPU time) on an UltraSparc 30 with a 300 MHz monoprocessor. However, this potential does

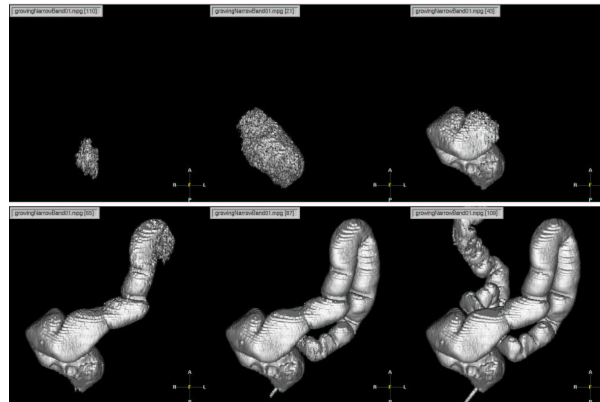


**Fig. 9.** Successive steps of front propagation inside the colon volume

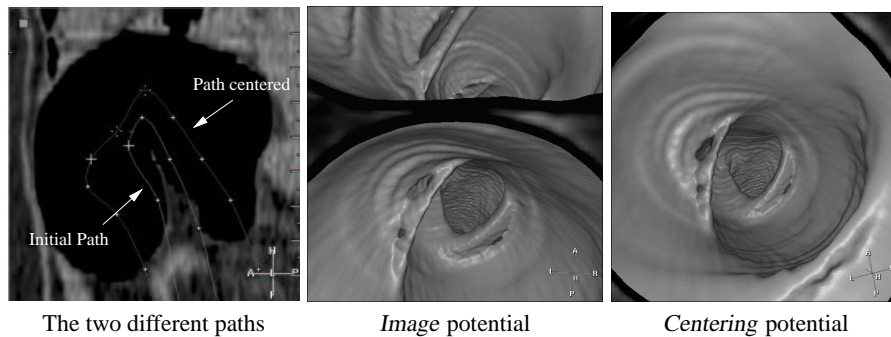


**Fig. 10.** Centering the path in the colon

not produce paths relevant for virtual endoscopy. Indeed, paths should remain not only in the anatomical object of interest but as far as possible from its edges. In order to achieve this target, we use the centering potential method as detailed in section 4. This approach needs a *shape* information. This information is provided by the previous front propagation. From its definition, the front sticks to the anatomical shapes as shown in figure 9. This is related to the use of Fast Marching algorithm to extract a surface for segmentation [3]. It gives a rough segmentation of the colon and provides a good

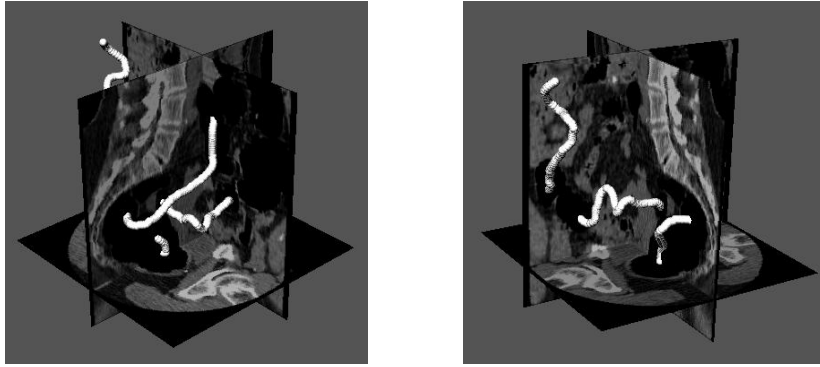


**Fig. 11.** 3D Views of a path inside the colon

information and a fast-reinitialization technique to compute the distance to the edges. Using this thresholded map as a potential that indicates the distance to the walls, we can correct the initial path as shown in figure 10-left. Both 3D paths are projected on the 2D slice for visualization. As expected, the new path remains more in the middle of the colon. The two different cross-sections in figures 10-middle and 10-right display the view of the interior of the colon from both paths at the u-turn shown in figure 10-left. This effect of centering the path enhances dramatically the rendering of the video sequence of virtual endoscopy obtained.<sup>1</sup> With the initial potential, the path is near the wall, and we see the u-turn, whereas with the new path, the view is centered into the colon, giving a more correct view of the inside of the colon.

Therefore, the two end points can be connected correctly, giving a path staying inside the anatomical object. The results are displayed in two 3D views in figure 11. But for virtual colonoscopy, it is often not necessary to set the two end points within the anatomical object.

### 5.3 Application to a Brain MRA Image

Tests were performed on brain vessels in a magnetic resonance angiography (MRA) scan. The problem is different, because there is only signal from blood. All other structures have been removed. The main difficulty here lies in the variations of the dye intensity. The path shown from two viewpoints tracks (see figure12) the superior sagittal venous canal, using a nonlinear function of the image dye intensity ( $P(x) = |I(x) - 100|^2 + 1$ ).

## 6 Conclusion

In this paper we presented a fast and efficient algorithm that computes a 3D path of minimal energy. This is particularly useful in medical image understanding for guiding endoscopic viewing.

<sup>1</sup>This video will be shown at the presentation, and is available at <http://www.ceremade.dauphine.fr/~cohen/ECCV00>.

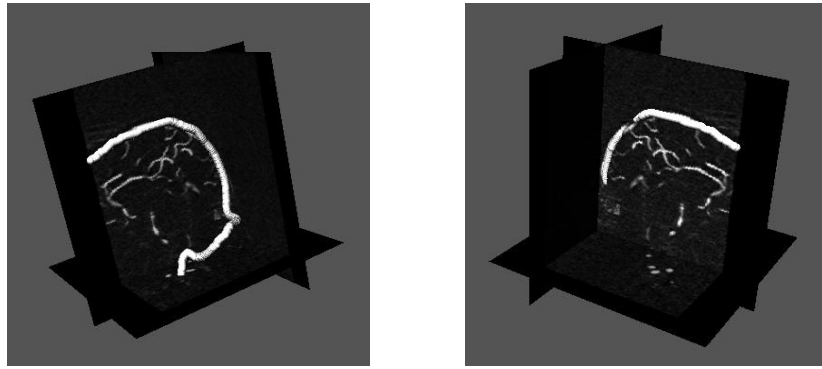


**Fig. 12.** Path tracking in brain vessels in a MR-Angiographic volume.

This work was the extension to 3D of a level-set technique developed in [1] for extracting paths in 2D images, given only the two extremities of the path and the image as inputs, with a front propagation equation.

We improved this front propagation equation by creating new algorithms which decrease the minimal path extraction computing cost, and reduce user interaction in the case of path tracking inside tubular structures. We showed that those techniques can be efficiently applied to the problem of finding a path in tubular anatomical structures for virtual endoscopy with minimum interactivity. In particular we extracted centered paths inside a CT dataset of the colon, and in a MR datasets of the brain vessels. We have proved the benefit of our method towards manual path construction, and skeletonization techniques, showing that only a few seconds are necessary to build a complete trajectory inside the body, giving only one or two end points and the image as inputs.

## References

1. Cohen, L.D., Kimmel, R.: Global Minimum for Active Contour Models: A Minimal Path Approach. *International Journal of Computer Vision*. **24** (1997) 57–78
2. Kass, M., Witkin, A., Terzopoulos, D.: Snakes: Active contour models. *International Journal of Computer Vision*. **4** (1988) 321–331
3. Malladi, R., Sethian, J.A.: A Real-Time Algorithm for Medical Shape Recovery. *Proceedings of International Conference on Computer Vision*. (1998) 304–310
4. Sethian J.A.: *Level set methods: Evolving Interfaces in Computational Geometry, Fluid Mechanics, Computer Vision and Materials Sciences*. Cambridge University Press (1999)
5. Rouy, E., Tourin, A.: A Viscosity Solution Approach to Shape-From-Shading. *SIAM Journal of Numerical Analysis*. **29** (1992) 867–884
6. Dijkstra, E.W.: A note on two problems in connection with graphs. *Numerische Mathematic*. **1** (1959) 269–271
7. McInerney, T., Terzopoulos, D.: Deformable Models in Medical Image Analysis, A Survey. *Medical Image Analysis*. **2** (1996)
8. Caselles, V., Kimmel, R., Sapiro, G.: Geodesic active contours. *Proceedings of International Conference on Computer Vision*. (1995) 694–699
9. Deschamps, T., Cohen, L.D.: Minimal path in 3D images and application to virtual endoscopy. *Les Cahiers du Cérémade, Université Paris Dauphine*. (2000)

10. Yeorong, G., Stelts, D.R., Jie, W., Vining, D.J.: Computing the centerline of a colon: a robust and efficient method based on 3D skeletons. Proceedings of IEEE Nuclear Science Symposium Conference Record. **23** (1993) 786–794
11. Chiu, R.C.H., Kaufman, A.E., Zhengrong, L., Lichan, H., Achiotou, M.: An interactive fly-path planning using potential fields and cell decomposition for virtual endoscopy. Proceedings of IEEE Nuclear Science Symposium Conference Record. **46** (1999) 1045–1049